Infrared Physics & Technology 132 (2023) 104753

Contents lists available at ScienceDirect

Infrared Physics and Technology

journal homepage: www.elsevier.com/locate/infrared

Regular article

Numerical study of light scattering and propagation in soymilk: Effects of particle size distributions, concentrations, and medium sizes

Hiroyuki Fujii *, Koyata Nishikawa, Hyeonwoo Na, Yuki Inoue, Kazumichi Kobayashi, Masao Watanabe

Division of Mechanical and Space Engineering, Faculty of Engineering, Hokkaido University, Kita 13 Nishi 8, Kita-ku, Sapporo, Hokkaido 060-8628, Japan

ARTICLE INFO

Keywords:
Light scattering and propagation in soymilk
Interference of electric fields
Dependent scattering theory
Radiative transfer theory
Near-infrared spectroscopy using scattered light

ABSTRACT

Understanding light scattering and propagation in soymilk is crucial for the nondestructive evaluation of food qualities of soymilk and its products by near-infrared spectroscopy. We aim to numerically examine light scattering and propagation in soymilk samples with different solid-content properties (particle size distributions and concentrations) and medium sizes. Using the dependent scattering theory, we calculated the light-scattering properties of the samples on the sub-nanometer scale. In contrast, we calculated light propagation on the millimeter scale using the radiative transfer theory. Our numerical results show that the scattering properties of soymilk strongly depend on the solid-content properties, implying a high correlation between the solid-content and scattering properties. The sample with the largest mean diameter and broadest size distribution has the smallest reduced scattering coefficient among the samples, although it has the largest scattering coefficient. We compared the reflected fluence rates in a cylinder and semi-infinite medium. The comparative study shows the finite size effect on light propagation can be negligible at the cylinder radius of more than 2.0 cm. In that case, the light propagation model for a semi-infinite medium is a better choice to provide fast calculations in inverse analysis on the scattering properties. Our findings are essential for further developing near-infrared spectroscopy using scattered light and the physics of light scattering in dense polydisperse media.

1. Introduction

Nondestructive evaluations of food qualities in soymilk and its products are crucial for controlling food production processes, such as the coagulation process of tofu (soybean curd) [1] and the dry process of soymilk powder [2]. The food qualities include hardness and sensory character [3], which relate to its structural and chemical properties. Soymilk is one of the colloidal suspensions, and its solid contents are dispersed in water. The main solid contents consist of protein, oil body, and carbohydrates. Properties of the solid content of soymilk, such as the particle size distribution and concentration, strongly correlate with the food qualities [4,5].

Near-infrared spectroscopy (NIRS) can potentially evaluate nondestructively food qualities related to its structure by assessing the solid-content properties. In the near-infrared wavelength (700–2000 nm), light is strongly scattered by the solid contents of soymilk. The protein and oil body sizes are 40 and 400 nm, respectively [1]. Because the optical wavelength is comparable to the particle size, the Mie scattering dominates in single-particle scattering. Moreover, soymilk is usually dense, so the electric fields scattered by the particles interact as interference. Light-scattering properties depend on the solid-content properties, expecting the applicability of NIRS using scattered light to evaluate the food qualities [6,7]. General NIRS has been widely used to evaluate chemical components for biological tissues and agricultural products based on the correlation between the chemical components and light-absorption properties [8,9]. Meanwhile, NIRS using scattered light is still under development and relies on the correlation between solid-content and light-scattering properties. For the NIRS development, elucidating light scattering and propagation in soymilk and its products is fundamental.

A few researchers have examined light scattering and propagation in soymilk and its products. Ringgenberg and coworkers have measured the photon mean free path (turbidity) of soymilk at different concentrations [10] and pH values [11] by diffuse wave spectroscopy. Saito and coworkers have evaluated the light-scattering properties of soymilk with coagulants to varying temperatures by spatially resolved diffuse reflectance measurements with the optical wavelength of 633 nm [6]. They recently examined light scattering in the optical wavelength range of 1300–1800 nm [7]. However, soymilk's light scattering and propagation still need to be clarified because of their complicated dependence on the solid-content properties, the optical wavelength, etc.

* Corresponding author.
E-mail address: fujii-hr@eng.hokudai.ac.jp (H. Fujii).

https://doi.org/10.1016/j.infrared.2023.104753
Received 19 March 2023; Received in revised form 20 May 2023; Accepted 20 May 2023
Available online 24 May 2023

The above studies have determined the light-scattering properties by inverse analysis of the light intensity measurements based on the radiative transfer theory (RTT). The RTT describes the light propagation on a millimeter scale and requires values of the scattering properties as physical parameters [12]. Meanwhile, the theoretical values of the scattering properties of soymilk using the electromagnetic theory (EMT) have yet to be investigated so far from the best of our knowledge. Because of the high size-polydispersity and high concentration of solid contents in soymilk, the calculation requires the EMT for polydisperse and dense suspensions on a sub-nanometer scale. The dependent scattering theory (DST) calculates the scattering properties for a dense suspension by treating the interference. The DST has been extensively employed for dense suspensions, e.g., silica and polystyrene [13–17] because the theory describes measurement data well. However, most previous works employed the monodisperse DST. The theoretical limitation makes it difficult to investigate light scattering in soymilk. In addition, because the theoretical values of the scattering properties are unknown, numerical studies of light propagation in soymilk using the RTT have yet to be reported. The numerical investigations are significant for suggesting adequate measurement conditions, such as a source-detector distance, medium size, etc., to determine the scattering properties by inverse analysis.

This paper aims to numerically examine light scattering and propagation in soymilk using the DST and RTT. Recently, we developed the DST for polydisperse suspensions [18] and showed nice agreements between the theoretical and experimental results for fat emulsions [19]. This study improves our numerical methods to calculate soymilk's light scattering and propagation. We confirmed the validity of our theoretical model by comparing the numerical results with published measurement data for soymilk samples. We investigate the influences of the size-polydispersity and concentration on the light-scattering properties in soymilk. Moreover, we suggest appropriate measurement conditions for light propagation in an inverse analysis of the scattering properties.

2. Models and methods

2.1. Multi-scale modeling of light scattering and propagation

We model light scattering and propagation in a soymilk sample based on a multi-scale approach, as shown in Fig. 1. On the microscopic scale (Fig. 1(a)), we consider the sample consists of discrete particles in a continuous background medium (water). On the scale compared to the optical wavelength, the EMT calculates the light-scattering properties, such as the scattering and reduced scattering coefficients (μ_s and μ_s'). On the macroscopic scale (Fig. 1(b)), the observation scale, we consider the sample as a continuous, so-called random medium, where the scattering properties continuously distribute. The RTT describes light propagation in a random medium on the scale. We incorporate the microscopic information, such as particle sizes, into the macroscopic light propagation model through the light-scattering properties.

The macroscopic scale categorizes into ballistic and diffusive scales. For the RTT, the radiative transfer equation (RTE) [20], a linear Boltzmann equation, is valid on both scales. Meanwhile, the diffusion equation (DE), obtained by the diffusion approximation (DA) to the RTE [21], is valid on the diffusive scale [22,23]. As shown in Fig. 1(b), μ_s and μ_s' quantify scattering events at the unit length in the ballistic and diffusive scales. In other words, they represent the reciprocal of the photon mean free paths.

2.2. Soymilk modeling

We considered three kinds of soymilk samples as a size-polydisperse system with a discrete particle size distribution. As for the size distribution, we refer to the data measured by Yamashita and Hirao using the dynamic light scattering technique [24]. They purchased soymilk

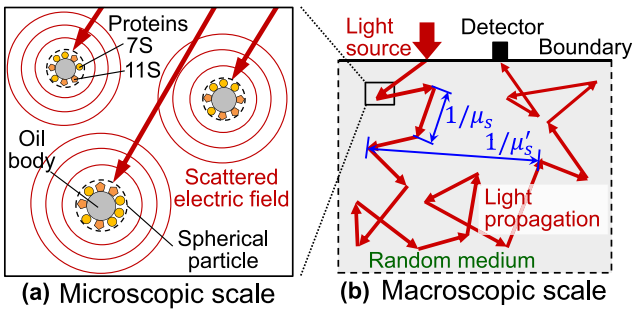

Fig. 1. Schematics of light scattering at a microscopic scale (~ 100 nm) and light propagation at a macroscopic scale (~ 10 mm) in the soymilk sample.

at a supermarket in Japan. The protein contents of original samples 1–3 are 8%, 11%, and 7%, respectively. We extracted the continuous scattering intensity distribution in the Ref. [24] as discrete data. Then, we modified the data based on a relation between the intensity and the particle fraction. We confirmed that the larger or smaller diameter fraction, which we do not consider, less influenced the results for the scattering properties. We used the truncated distributions without the whole range distribution to reduce the computational costs of the light-scattering properties using the EMT. Fig. 2 shows the particle size distributions of the three samples in the logarithmic Gaussian form. Here, the particle fraction is normalized so that the summation with the particle sizes is unity. In soymilk, the proteins (e.g., 7S and 11S) agglomerate to the oil body at a certain probability under an unheated condition. The reference data considers the protein and oil body aggregate as spherical particles (please see Fig. 1(a)). This study assumed the size distribution to be unchanged by varying concentrations. Samples 1-3' mean diameters are 467 nm, 562 nm, and 677 nm, respectively. These values are about twice or three times as large as Intralipid-20% (intravenous fat emulsion, mean diameter of 214 nm) [25]. The fact means the forward scattering is more prominent in soymilk over the fat emulsion. As shown in Fig. 2, the particle size distribution of soymilk varies by sample (manufacturer). This variation differs from silica suspensions and intravenous fat emulsions. This fact motivates us to examine the influence of the variation on light scattering and propagation in soymilk. Generally, its peak value will be reduced when a particle size distribution is broadened. The peak values of the size distributions for samples 1–3 are 0.136, 0.142, and 0.107, respectively. The phenomenon is found between samples 1 and 3 or 2 and 3. However, we do not clearly find the phenomenon between samples 1 and 2; the peak values are almost identical. This fact means the distribution shapes are similar to samples 1 and 2, but the distribution is shifted to a larger diameter for sample 2.

We modeled the soymilk particles as hard spheres. Although the validation of the hard-sphere interaction has yet to be confirmed sufficiently in soymilk, extensive studies have demonstrated the validation in other similar systems, such as fat emulsion [19] and milk [26].

2.3. Dependent and independent scattering theories (DST and IST)

We consider the EMT for a size-polydisperse system with N_d-kinds of particle diameters. The total number of the particles N for the system is given as $\sum_{\alpha=1}^{N_d} N_\alpha$, and N_α is the total number of particles for the α-class of diameter d_α ($\alpha = 1, 2, \ldots, N_d$).

The dependent scattering theory (DST) as the EMT calculates the scattering properties for dense colloidal suspensions [18,27]. The polydisperse DST treats the interference of different particle-diameter classes, denoted as α and $\beta(= 1, 2, \ldots, N_d)$ [18]. For the polydisperse DST, the phase function, representing the collective scattering behavior in a many-particle system, is given as

$$P^{DP}(\theta,\phi) = \sum_{\alpha=1}^{N_d}\sum_{\beta=1}^{N_d} \sqrt{n_\alpha n_\beta}\, \boldsymbol{F}_\alpha^{Mie}(\theta,\phi)\cdot \boldsymbol{F}_\beta^{Mie*}(\theta,\phi) S_{\alpha\beta}(\theta), \quad (1)$$

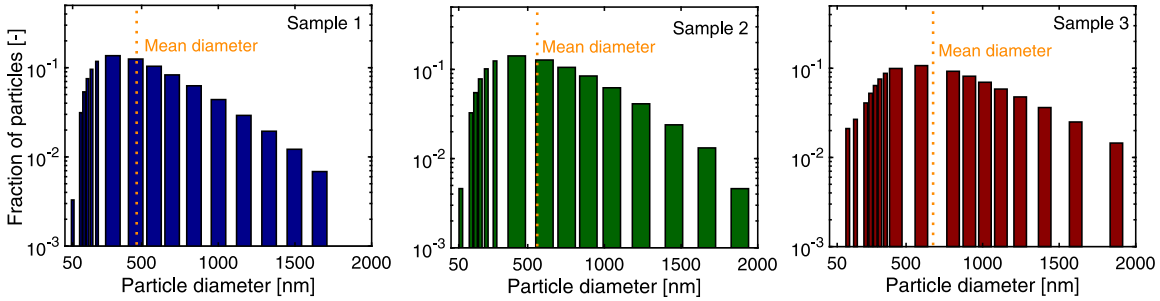

Fig. 2. Particle size distributions of the three soymilk samples based on the Ref. [24]. The fraction is normalized so that the summation with the particle sizes is unity.

where θ is the polar angle and set to the scattering angle; ϕ is the azimuthal angle; $n_\alpha = N_\alpha/V$ or $n_\beta = N_\beta/V$ is the number density for the α-class or the β-class of particle diameters; $\boldsymbol{F}_\alpha^{Mie}(\theta,\phi)$ is the scattering amplitude vector using the Mie theory based on the associated Legendre and Riccati-Bessel functions [28,29]; $\boldsymbol{F}_\beta^{Mie*}(\theta,\phi)$ is the complex conjugate of $\boldsymbol{F}_\beta^{Mie}(\theta,\phi)$; and $S_{\alpha\beta}(\theta)$ is the partial static structure factor, representing the interference of the scattered fields between the different diameter classes. In the calculation of $S_{\alpha\beta}(\theta)$, we used the polydisperse Percus–Yevick model, which is a hard-sphere model to treat many-body correlations between particles [30,31]. Using Eq. (1), we calculate the light-scattering properties. Please see our previous paper [18] for explicit formulations of the scattering properties.

To examine the effects of the interference on the scattering properties, we employ the independent scattering theory (IST), which does not treat the interference, unlike the DST. We can derive the IST for a polydisperse system from the DST once we consider $S_{\alpha\beta}(\theta)$ as $\delta_{\alpha\beta}$, where $\delta_{\alpha\beta}$ denotes the Kronecker delta function. To examine the polydisperse effect, we employ the monodisperse DST and IST. For the monodisperse theories, please see the Refs. [14,15,27].

Comparative studies have shown that the DST nicely describes the experimental data of the scattering properties for various colloidal suspensions, such as polystyrene [15,16], silica [14], and fat emulsion [19]. However, a comparative study for soymilk has been little reported. Section 3.2 discusses the comparative analysis of soymilk.

2.4. Numerical conditions of the DST and IST

We varied volume fractions $\eta[-]$ of the soymilk particles; 0.01, 0.02, ⋯ 0.20 mimicking dilutions by water and condensations by water evaporation. We set the optical wavelength of 780 nm in the near-infrared region. The optical wavelength is the same as a solid-state laser (Calmar Laser). Based on the reference data of soybean oil fat emulsions [32], we consider the particle and water refractive indices as 1.467 and 1.327, respectively, for soymilk samples. The value for the particle is close to another reference data of 1.46 [4]. Although not shown here, we examined the sensitivity of the reduced scattering coefficients on the refractive indices of particles: 1.46, 1.47, and 1.48. We found that the difference in the reduced scattering coefficient from the result at 1.47 is approximately 20% at the volume fraction of 20%. This result suggests that the accurate determination of particle refractive index is crucial. Generally, the imaginary part of the particles' complex refractive index is negligibly smaller than the real part. This study considers only the real part, the same as previous works [4,32]. The polydisperse system treats the particle size distribution, while the monodisperse system uses the mean diameter.

2.5. Radiative transfer and diffusion equations (RTE and DE)

This study considered the time-dependent RTE and DE for the time-domain NIRS [33]. For the formulations of the RTE and DE, refer to the Ref. [33]. We employed the analytical solutions of the RTE and DE in a 3D semi-infinite homogeneous medium, as shown in Fig. 3(a). The

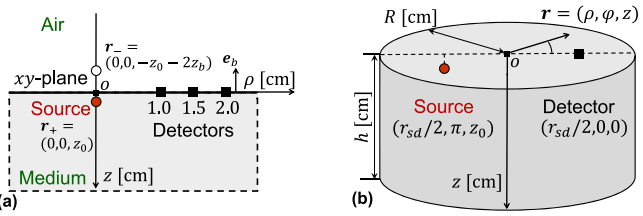

Fig. 3. Schematic of the random media: (a) semi-infinite medium and (b) cylinder.

comparative study of the RTE and DE examined a condition where the DA holds. Moreover, we employed the solutions of the DE in a homogeneous cylinder, as shown in Fig. 3(b). As an experiment, this study assumed the time-domain measurement of light intensity for soymilk in a beaker on a magnetic stirrer. In such a condition, examining the finite-size effect on light propagation is crucial for accurate and efficient experiments. In an experiment of the light-scattering properties by inverse analysis, we need to know prior information, such as an appropriate distance between the source and detector, container size, etc. Hence, this study considers the cylindrical geometry. Here, we model the light propagation in a cylindrical tank fulfilled by soymilk. The comparative study for the semi-infinite medium and cylinder examined the finite size effect on light propagation. Light reflection and refraction occur at a medium-air interface due to a difference in the refractive indices between the medium and air. The refractive index mismatch boundary conditions treat these phenomena [34,35].

2.6. Analytical solutions in a semi-infinite medium for the RTE and DE

We constructed the analytical solution of the RTE in a semi-infinite medium by the solution in an infinite medium based on the method of images [36]. When an isotropic point source is an incident at the origin of the Cartesian ($\boldsymbol{r} = (x, y, z)$) and initial time, the analytical form of the fluence rate for the RTE in an infinite medium at time t is given [37]

$$\boldsymbol{\Phi}_{RTE}^{inf}(r,t) = \boldsymbol{\Phi}_{LK}(r,t;\mu_a,\mu_s,\boldsymbol{\sigma}_p,n), \tag{2}$$

where $r = |\boldsymbol{r}|$ and $\boldsymbol{\Phi}_{LK}$ represents the analytical form by Liemert and Kienle based on the spherical Bessel function of the first kind. μ_a and n denote the absorption coefficient and refractive index of soymilk. $\boldsymbol{\sigma}_p$ is the expansion coefficient vector of the normalized phase function by Legendre polynomials up to a maximum order of N_L. Several independent studies have confirmed the verification of the solution [38,39]. The original open-source code of $\boldsymbol{\Phi}_{LK}$ employs the Henyey–Greenstein function as the normalized phase function. In this study, we modified the code to use the phase function of the DST. Moreover, we modified the code to adopt the delta-Eddington (dE) method to provide more stable solutions [40]. Soymilk samples are highly forward scattering media, where the normalized phase function is very sharp at a small scattering angle. In the accurate calculations of the sharp-shaped phase function, we employed the dE method. But,

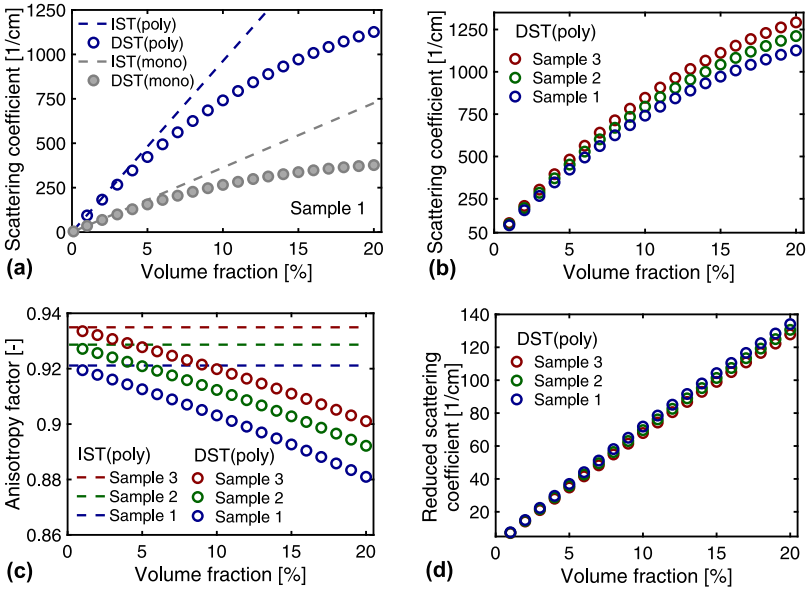

Fig. 4. Volume-fraction dependence of the scattering properties using the DST and IST: (a) scattering coefficients μ_s using the polydisperse and monodisperse; (b) scattering coefficients, (c) anisotropy factors g, and (d) reduced scattering coefficients μ_s' in the three soymilk samples.

we extended the technique to treat the phase function calculated from the DST. We decomposed the phase function using the DST into the delta-function component and other components. Then, we further decomposed the other components into the Legendre polynomials up to the 50th order. We confirmed the results almost unchanged when the higher order is treated in calculations. Summing the solutions in an infinite medium over different distances, we obtain the analytical form of the RTE in a semi-infinite medium

$$\Phi_{RTE}^{semi}(\boldsymbol{r},t;z_0,z_b)=\Phi_{RTE}^{inf}(|\boldsymbol{r}-\boldsymbol{r}_+|,t)-\Phi_{RTE}^{inf}(|\boldsymbol{r}-\boldsymbol{r}_-|,t), \tag{3}$$

where $\boldsymbol{r}=(\rho,z)$, $\boldsymbol{\rho}=(x,y)$, a real source position of $\boldsymbol{r}_+=(0,0,z_0)$ with $z_0=1/\mu_s'$, an imaginary source position of $\boldsymbol{r}_-=(0,0,-z_0-2z_b)$ with $z_b=\gamma(n)D$ (Fig. 3(a)). $\gamma(n)$ represents the coefficient for the diffusive reflection [41] depending on the refractive index n of the medium and $\boldsymbol{e}_b$ represents the outward normal unit vector at the boundary. $D=1/(3\mu_s')$ represents the photon diffusion coefficient. The source-detector (SD) distance, r_{sd}, is given by $|\boldsymbol{r}-\boldsymbol{r}_+|$. In this paper, we used the exact solution of the RTE for an infinite medium while employing the DA on the refractive index mismatch boundary condition. Several studies have confirmed the verification of the DA on the boundary by the numerical solutions of the RTE [42] and Monte Carlo simulations [43].

In the same way of Φ_{RTE}^{semi}, we obtain the analytical form of the fluence rate for the DE in a semi-infinite medium [44]

$$\Phi_{DE}^{semi}(\boldsymbol{r},t;z_0,z_b)=\frac{v}{(4\pi Dvt)^{3/2}}e^{-\mu_a vt}\left[e^{-\frac{|\boldsymbol{r}-\boldsymbol{r}_+|^2}{4Dvt}}-e^{-\frac{|\boldsymbol{r}-\boldsymbol{r}_-|^2}{4Dvt}}\right], \tag{4}$$

where v is the light velocity in the medium.

2.7. The DE solution in a cylinder

The analytical solution of the DE for a homogeneous cylinder with a radius of R and height h is given in the cylindrical coordinate $\boldsymbol{r}=(\rho,\varphi,z)$ (Fig. 3(b)) [45]

$$\begin{aligned}&\Phi_{DE}^{cyl}(\boldsymbol{r},t;z_0,z_b)\\&=\frac{1}{2\pi R'^2}\sqrt{\frac{v}{\pi Dt}}e^{-\mu_a vt}\sum_{k=-N_s}^{N_s}\left[e^{-\frac{(z-z_{1k})^2}{4Dvt}}-e^{-\frac{(z-z_{2k})^2}{4Dvt}}\right]\\&\times\sum_{m=-N_s}^{N_s}\cos(m\varphi-m\varphi_0)\sum_{l=1}^{N_s}e^{-Dvs_l^2t}J_m(s_l\rho_0)J_m(s_l\rho)J_{m+1}^{-2}(R's_l)\end{aligned} \tag{5}$$

with the source position (ρ_0,φ_0,z_0) and $R'=R+z_b$. N_s is the number of the summations with the integers k, m, and l (e.g., $k=0,\pm1,\pm2,\ldots,\pm N_s$). The N_s-value is theoretically infinite, and we set it 100 in numerical calculation. $z_{1k}=2kh+z_0+4kz_b$ and $z_{2k}=2kh-z_0+(4k-2)z_b$ correspond to positive and negative sources, respectively. J_m represents the Bessel function of the first kind and mth order. s_l are the positive roots of J_m divided by R', satisfying $J_m(s_lR')=0$. We fixed the height of $h=3.0$ cm while we considered three cases of the cylinder radius: $R=1.5$ cm, 2.0 cm, and 2.5 cm. We set the source and detector positions so that the midpoint between them is the origin of the coordinates, as shown in Fig. 3(b).

2.8. Numerical conditions of the analytical solutions

In the RTE solution, we used the scattering coefficient and normalized phase function, μ_s and $\hat{p}$, by the DST. In the DE solution, meanwhile, we used the reduced scattering coefficient μ_s' by the DST. We consider the absorption coefficient 0.1 cm^{-1} in all the cases. The value is in the same order in the previous study [6]. We calculated the analytical solution by MATLAB up to 6000 ps at different SD distances of 1.0 cm, 1.5 cm, and 2.0 cm. The computational times for Φ_{RTE}^{semi}, Φ_{DE}^{semi}, and Φ_{DE}^{cyl} at each SD distance, volume fraction, and sample are approximately 4 min, 2 s, and 1 min, respectively.

3. Results and discussion

3.1. Light scattering properties

We numerically examined the volume-fraction dependence of the scattering properties in the soymilk samples. Fig. 4(a) shows the scattering coefficients in sample 1 using the four theories: monodisperse IST, polydisperse IST, monodisperse DST, and polydisperse DST. The reciprocal of the scattering coefficient represents the photon mean free path in the ballistic region. At a low volume-fraction region (approximately below 5%), the IST and DST results agree with each other for each system and show a linear trend of the volume-fraction dependence. This result means that the interference of the scattered fields little influences the scattering coefficient. At the high volume-fraction region, both theories' results disagree. The DST result shows a curve trend and becomes smaller than the IST, indicating the enhancement of the destructive interference. Comparing the polydisperse results with

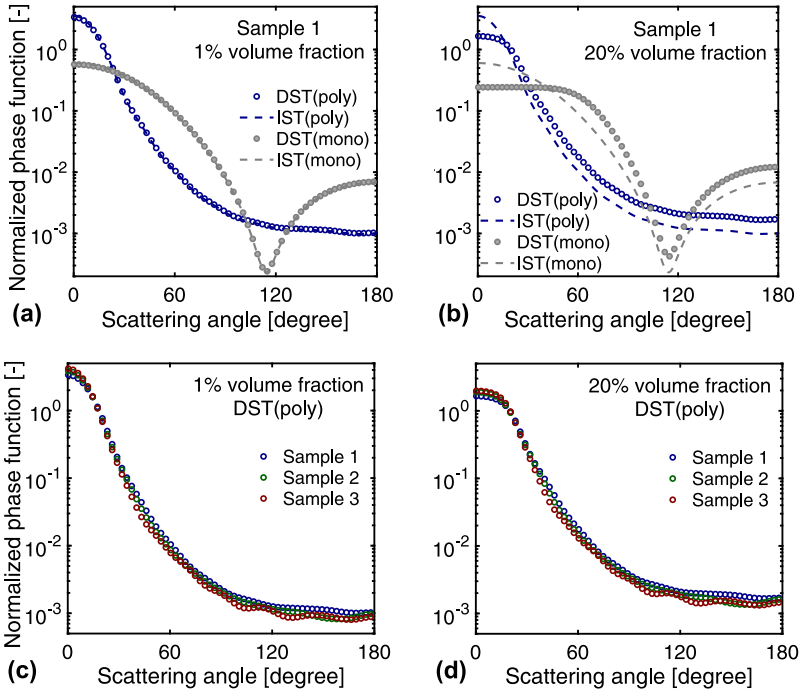

Fig. 5. Normalized phase functions: the four theories in sample 1 at (a) 1% and (b) 20% volume fractions; the polydisperse DST in the three samples at (c) 1% and (d) 20% volume fractions.

the monodisperse results shows the strong influence of the particle size distribution on the scattering coefficient. Although not shown here, we have confirmed the strong influences of the size polydispersity on the other scattering properties.

Fig. 4(b) compares the scattering coefficients for different soymilk samples using the polydisperse DST. The results for sample 3 are the largest among the three samples because of the largest mean diameter and broadest size distribution, as shown in Fig. 2.

We examined the anisotropy factors, g, at different volume fractions and samples in Fig. 4(c). The anisotropy factor represents the degree of anisotropy of light scattering ($-1 \leq g \leq 1$). The cases of $g = 1$, 0, and -1 mean the purely forward, isotropic, and purely backward scattering, respectively. Fig. 4(c) shows the g-values are above 0.88 for all the cases, meaning that the soymilk samples are highly forward-scattering media. The g-values of soymilk samples are more significant than those of Intralipid-20% (approximately $0.8 > g > 0.6$) [19]. Because of the interference, the anisotropy factors decrease as the volume fraction increases, suppressing the forward scattering. The IST results are independent of the volume fraction. Like the scattering coefficient, sample 3 has the largest values among the samples.

As shown in Fig. 4(d), the volume-fraction dependence of the reduced scattering coefficient, μ_s', has a curve trend similar to the scattering coefficient, μ_s. The inverse of μ_s' represents the photon mean free path the same as μ_s but in the diffusive region. However, the curvature for μ_s' is smaller than that for μ_s, meaning the weaker interference effects in the diffusive region of light propagation. Unlike the μ_s-results, sample 3 has the smallest μ_s'-values. This result is non-trivial because, generally, the medium with a larger particle size scatters light more strongly, and the strength is more significant. The result comes from the following reason. The reduced scattering coefficient is given as $\mu_s' = (1-g)\mu_s$, and sample 3 has the smallest value of $1-g$. The smallest value dominates over the largest μ_s-value in μ_s'. The average differences in μ_s' between samples based on the value of sample 2 are 2/cm at the volume fraction of 10% and 3/cm at 20%. Examining whether the difference can be found in experiments in future work is significant.

Figs. 5(a) and (b) compare the normalized phase functions using the four theories in sample 1 at the volume fractions of 1% and 20%, respectively. The normalized phase function satisfies the condition that the summation of the phase function over the whole solid angle is unity. At the volume fraction of 1%, the DST results coincide with the IST results in the whole angle range, indicating little interference effect. Meanwhile, at the volume fraction of 20%, the results of both theories disagree with each other. The interference effect suppresses the forward scattering (the scattering angle region of 0–20 degrees), accordingly increasing the backward scattering (the angle region of 120–180 degrees). Figs. 5(c) and (d) compare the results using the polydisperse DST in the three samples. Although the results differ from each sample, the difference among the samples does not strongly depend on the volume fraction. That is the reason for the less volume-fraction dependence of the differences in g among the samples (Fig. 4(c)), where g is the average cosine of the normalized phase function.

3.2. Comparison with measurement data of the scattering properties

To validate our numerical calculations using the polydisperse DST, we compared the numerical results with measurement data of the scattering properties in soymilk by Ringgenberg and coworkers [10]. They measured the concentration dependence of the photon mean free path at the optical wavelength of 532 nm for two soymilk samples: 4% and 5% protein contents by diffusing wave spectroscopy. Although they have not shown the particle size distributions of the two samples, they evaluated the particle diameters: the apparent particle diameter of 178 nm by dynamic light scattering technique, while the mean diameter of 850 nm by a monodisperse DST fitting. The large difference in the diameters suggests the broadness of the particle size distribution of the samples. The diameter values are within the size distribution for our current samples. From the measurement data of the photon mean free path, we obtained the data of the reduced scattering coefficient by assuming the absorption coefficient of 1.0 cm^{-1}, larger than the value at the wavelength of 780 nm. The assumption is based on the fact that the optical absorbance of soymilk at the wavelength of 532 nm is larger than that at 780 nm [2]. We calculated the reduced scattering coefficient by the polydisperse DST for samples 1-3 at the wavelength of 532 nm and the particle refractive index of 1.39, the

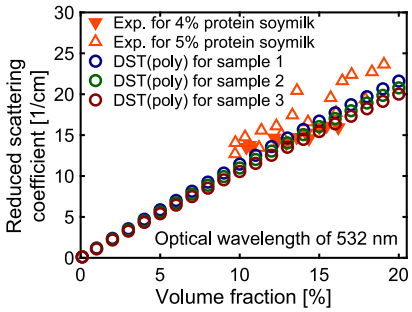

Fig. 6. Comparisons of our calculations using the polydisperse DST with measurement data by Ringgenberg and coworkers [10] at the optical wavelength of 532 nm for two soymilk samples: 4% and 5% protein contents.

same as the Ref. [10]. Fig. 6 shows the numerical results agree with the experimental results, suggesting the validation of our numerical calculations.

3.3. Fluence rate

We examined the DA from the temporal profiles of the fluence rate using the RTE and DE for a semi-infinite medium (Eqs. (3) and (4)). Fig. 7(a) shows the temporal profiles at the volume fraction of 1% for the SD distances of 1 cm and 2 cm in sample 1. The RTE profiles differ from the DE profiles, especially at the short distance of 1 cm, although the profiles using both equations are similar. The result means the DA is invalid at the condition, and the light remains ballistic. As shown in Fig. 7(b), the profiles using both equations agree at the volume fraction of 10%. This result suggests the DA holds, and the light is diffusive. Extensive studies have shown that the DA generally holds on a scale longer than the characteristic length of $10/(\mu_s' + \mu_a)$ [22,35,46]. Because $1/(\mu_s' + \mu_a)$ represents the photon mean free path, the characteristic length means that the light becomes diffusive after approximately ten times of scattering and absorption processes. In sample 1, the characteristic lengths are 1.31 cm at the volume fraction of 1% and 0.14 cm at 10%, respectively, consistent with our current results. Fig. 7(c) compares the temporal profiles in the three samples using the RTE at the volume fractions of 1% and 10%. The profiles differ between the samples, but the differences are not significant. This result is because of the insignificant difference in the μ_s'-values between the samples (please see Fig. 4(d)).

We evaluated a mean absolute percentage difference (MAPD) of the fluence rate, D_{Φ}, between the RTE and DE for a semi-infinite medium

$$D_{\Phi}(\Phi_{RTE}^{semi}, \Phi_{DE}^{semi}) = \frac{1}{M_2 - M_1} \sum_{m=M_1}^{M_2} \left| \frac{\hat{\Phi}_{RTE}^{semi}(t_m) - \hat{\Phi}_{DE}^{semi}(t_m)}{\hat{\Phi}_{RTE}^{semi}(t_m)} \right| \times 100, \quad (6)$$

where $\hat{\Phi}_{RTE}^{semi}$ and $\hat{\Phi}_{DE}^{semi}$ represent the fluence rates normalized by their peak values using the RTE and DE, respectively. The summation with respect to the timestep m is over the time period from the timestep M_1 when $\hat{\Phi}_{RTE}^{semi}$ rises to $10^{-1.0}$ before the peak to the timestep M_2 when $\hat{\Phi}_{RTE}^{semi}$ decays to $10^{-1.5} \simeq 0.032$ after the peak. For the details of the summation, please refer to our previous work [39]. We discuss MAPDs [%] in sample 1 because the other samples have the same trends. Fig. 7(d) shows MAPD [%] decreases as the volume fraction increases because of the increases in μ_s' and the reduction in the characteristic length of $10/(\mu_s' + \mu_a)$. MAPDs are over 4% at the volume fraction of 1%, while MAPDs are less than 4% at the other conditions. This result means the DA holds at a volume fraction of more than 2%.

We examined the finite size effects on the light propagation by comparing the DE solutions in the cylinder and semi-infinite medium (Eqs. (4) and (5)). Here, we show the results in sample 1 because the results in the other samples are similar. Fig. 8(a) compares the normalized fluence rates at the volume fraction of 1% and the cylinder radius of $R = 1.5$ cm. The results for the two media coincide at the SD distance of 1.0 cm. Meanwhile, at the SD distance of 2.0 cm, the profile for the cylinder decays faster than that for the semi-infinite medium, suggesting the finite size effect. The distance between the detector and the nearest boundary is 1.0 cm in the SD distance of 1.0 cm and 0.5 cm in the SD distance of 2.0 cm, respectively. The finite medium size suppresses the light propagation and does not allow the reentry of the light from outside of the medium. This effect decreases the fluence rate at a longer time, corresponding to a longer photon path length. Figs. 8(b) and (c) correspond to the cases of a larger cylinder radius and a larger volume fraction, respectively. The finite size effect less influences the fluence rates for the two cases. In the latter case (higher μ_s'-values), photons are trapped inside the medium due to light scattering.

We evaluated the MAPD between the cylinder and semi-infinite medium

$$D_{\Phi}(\Phi_{DE}^{cyl}, \Phi_{DE}^{semi}) = \frac{1}{M_2 - M_1} \sum_{m=M_1}^{M_2} \left| \frac{\hat{\Phi}_{DE}^{cyl}(t_m) - \hat{\Phi}_{DE}^{semi}(t_m)}{\hat{\Phi}_{DE}^{cyl}(t_m)} \right| \times 100, \quad (7)$$

where $\hat{\Phi}_{DE}^{cyl}$ represents the normalized fluence rates for the cylinder. The other details are the same as Eq. (6). Here, we focus on the results at the SD distance of 2.0 cm, where the DA holds for a semi-infinite medium at all the volume fractions. Then, the finite size only contributes to the photon path longer than the SD distance. The reason is to find the condition where the DE for a semi-infinite medium is applicable. Fig. 8(d) shows that MAPDs become smaller at a larger cylinder radius and larger volume fraction. From the figure, the finite size effect can be negligible when the cylinder radius is more than 2.0 cm because MAPDs are less than 5% in most of cases.

4. Conclusions

We numerically examined light scattering and propagation using the EMT and RTT in soymilk samples at different size distributions and concentrations. We modeled the soymilk sample as a dense polydisperse suspension and the solid contents as hard spheres. We obtained the following conclusions. First, the light-scattering properties of soymilk strongly depend on the size-polydispersity and concentration of solid contents, implying the high correlation between the solid-content and scattering properties. The results suggest that theoretical investigations for soymilk must treat the size-polydispersity, although most previous research did not treat it. When nondestructive evaluation of the solid-content properties in soymilk is conducted by inverse analysis using the EMT, our numerical method based on the polydisperse DST is a great candidate for the accurate evaluation because the monodisperse theory, used in previous works, does not treat the nature of the solid contents.

Second, sample 3, with the largest mean diameter and broadest size distribution, has the smallest reduced scattering coefficient, while the sample has the largest scattering coefficient. This nontrivial result can be explained by the largest anisotropy factor, meaning the highest forward scattering. Third, the DA holds at a volume fraction larger than 1%, and the finite size effect on light propagation can be negligible when the cylinder radius is more than 2.0 cm. In those cases, the DE solution for a semi-infinite medium is the best choice for fast and accurate calculations of light propagation in inverse analysis of the scattering properties.

This study aimed to find when the DE for a semi-infinite medium is applicable. Hence, we focused on the large-sized medium. Meanwhile, the smaller-sized medium is better for sample preparation in actual measurements. In the smaller-sized medium, the DE breaks down. The numerical examination of light propagation for small-sized media using the RTE is significant in future work. Our findings are indispensable for developing NIRS using scattered light that evaluates the food qualities of soymilk and its product related to the structure throughout assessing the solid-content properties. We compared our calculations

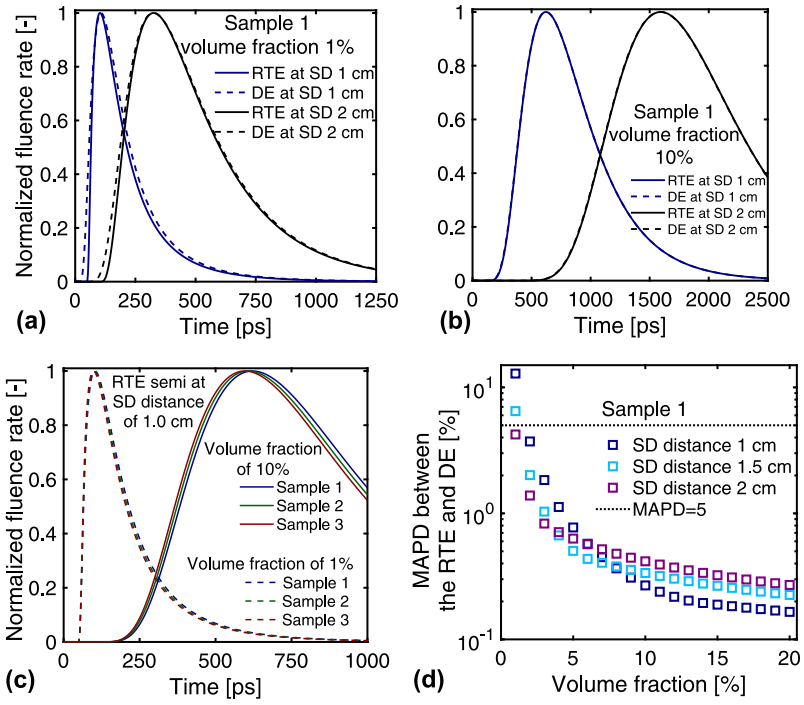

Fig. 7. Temporal profiles of the fluence rate using the RTE and DE for a semi-infinite medium, normalized by the peak value. The results for the volume fractions of (a) 1% and (b) 10% at the SD distances of 1 cm and 2 cm in sample 1; (c) comparisons of the RTE results in the three samples at the volume fractions of 1% and 10%; (d) the mean absolute percentage difference (MAPD) of the profiles between the RTE and DE (Eq. (6)) at different SD distances in sample 1.

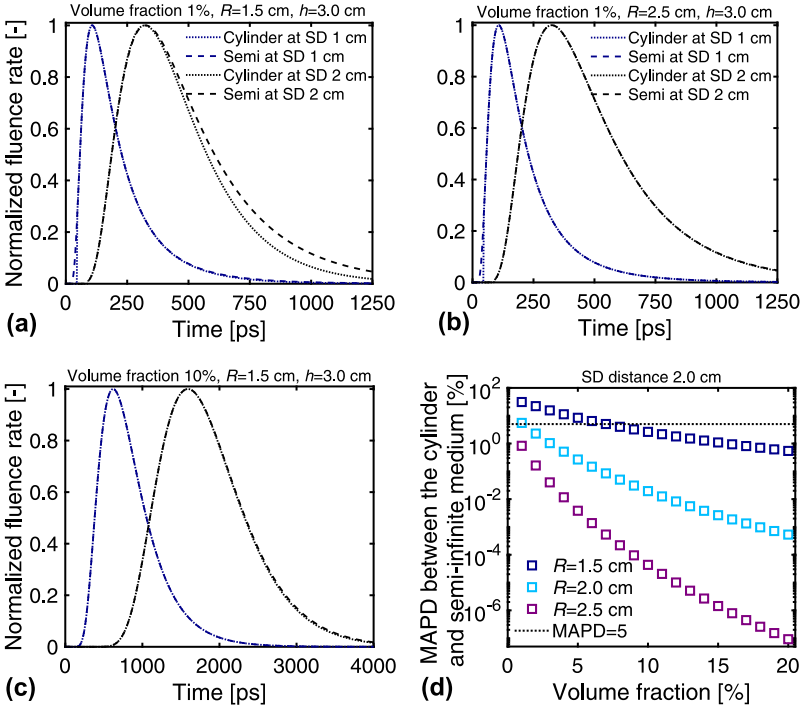

Fig. 8. (a-c) Temporal profiles of the normalized fluence rate using the DE for a cylinder and semi-infinite medium in sample 1 at the three cases of the volume fraction and cylinder radius R. (d) MAPD between the cylinder and semi-infinite medium (Eq. (7)) at different radii in sample 1. The line for MAPD of 5% is plotted.

with experimental data by Ringgenberg and coworkers. To the best of our knowledge, their work is the only one that measures the volume fraction dependence of the light-scattering properties of soymilk. In future work, an experimental study of the light scattering properties of soymilk and further comparative studies are necessary to validate the numerical modeling of soymilk. Our findings are also essential for

the other research fields of light-scattering phenomena, such as light scattering in fogs and clouds for remote sensing [47–50].

CRediT authorship contribution statement

Hiroyuki Fujii: Conceptualization, Software, Investigation, Funding acquisition, Writing – original draft. **Koyata Nishikawa:** Conceptualization, Formal analysis, Investigation, Writing – review & editing. **Hyeonwoo Na:** Software, Formal analysis, Investigation, Writing – review & editing. **Yuki Inoue:** Methodology, Software, Investigation, Writing – review & editing. **Kazumichi Kobayashi:** Writing – review & editing, Supervision. **Masao Watanabe:** Writing – review & editing, Supervision.

Declaration of competing interest

The authors declare the following financial interests/personal relationships which may be considered as potential competing interests: Hiroyuki Fujii reports financial support was provided by Takano Life Science Research Foundation. Hiroyuki Fujii reports financial support was provided by Japan Society for the Promotion of Science, KAKENHI.

Data availability

Data will be made available on request.

Acknowledgments

The authors would like to thank Dr. G. Nishimura for his fruitful comments from the experimental point of view. The authors also thank Dr. Y. Yamashita and Ms. T. Sekine at the Chiba Institute of Science for allowing us to use their data on the particle size distribution of soymilk. The first author (H.F.) acknowledges support from Takano Life Science Research Foundation, Japan, Grant-in-Aid for Scientific Research (22KK0243, 20H02076 and 21H05577) of the Japan Society for the Promotion of Science, KAKENHI.

References

[1] Y. Chen, T. Ono, Protein particle and soluble protein structure in prepared soymilk, Food Hydrocoll. 39 (2014) 120–126.
[2] X. Chen, X. Lei, Application of a hybrid variable selection method for determination of carbohydrate content in soy milk powder using visible and near infrared spectroscopy, J. Agric. Food Chem. 57 (2) (2009) 334–340.
[3] L. Ma, B. Li, F. Han, S. Yan, L. Wang, J. Sun, Evaluation of the chemical quality traits of soybean seeds, as related to sensory attributes of soymilk, Food Chem. 173 (2015) 694–701.
[4] A. Malaki Nik, S.M. Tosh, L. Woodrow, V. Poysa, M. Corredig, Effect of soy protein subunit composition and processing conditions on stability and particle size distribution of soymilk, LWT - Food Sci. Technol. 42 (7) (2009) 1245–1252.
[5] Z. Yan, L. Zhao, X. Kong, Y. Hua, Y. Chen, Behaviors of particle size and bound proteins of oil bodies in soymilk processing, Food Chem. 194 (2016) 881–890.
[6] Y. Saito, K. Konagaya, T. Suzuki, N. Kondo, Determination of optical coefficients of tofu using spatially resolved diffuse reflectance at 633 nm, Eng. Agric. Environ. Food. 11 (1) (2018) 38–42.
[7] Y. Saito, T. Suzuki, N. Kondo, Evaluation of optical properties of tofu samples produced with different coagulation temperatures and times using near-infrared transmission spectroscopy, Infrared Phys. Technol. 123 (2022) 104149.
[8] V. Ntziachristos, Going deeper than microscopy: The optical imaging frontier in biology, Nature Methods 7 (8) (2010) 603–614.
[9] J. Qin, R. Lu, Measurement of the optical properties of fruits and vegetables using spatially resolved hyperspectral diffuse reflectance imaging technique, Postharvest Biol. Technol. 49 (3) (2008) 355–365.
[10] E. Ringgenberg, M. Corredig, M. Alexander, Physico-chemical characterization of soymilk particles as a function of their volume fraction: Comparison with theoretical systems, Food Biophys. 7 (2012) 244–257.
[11] E. Ringgenberg, M. Alexander, M. Corredig, Effect of concentration and incubation temperature on the acid induced aggregation of soymilk, Food Hydrocoll. 30 (2013) 463–469.
[12] F. Long, F. Li, X. Intes, S.P. Kotha, Radiative transfer equation modeling by streamline diffusion modified continuous Galerkin method, J. Biomed. Opt. 21 (3) (2016) 036003.
[13] Y. Yamada, J.D. Cartigny, C.L. Tien, Radiative transfer with dependent scattering by particles: Part 2 - experimental investigation, J. Heat Transf. 108 (1986) 614–618.
[14] V.D. Nguyen, D.J. Faber, E. van der Pol, T.G. van Leeuwen, J. Kalkman, Dependent and multiple scattering in transmission and backscattering optical coherence tomography, Opt. Express 21 (24) (2013) 29145–29156.
[15] S. Fraden, G. Maret, Multiple light scattering from concentrated, interacting suspensions, Phys. Rev. Lett. 65 (4) (1990) 512–515.
[16] L.F. Rojas-Ochoa, S. Romer, F. Scheffold, P. Schurtenberger, Diffusing wave spectroscopy and small-angle neutron scattering from concentrated colloidal suspensions, Phys. Rev. E 65 (2002) 051403 1–8.
[17] M.I. Mishchenko, Asymmetry parameters of the phase function for densely packed scattering grains, J. Quant. Spectrosc. Radiat. Transf. 52 (1) (1994) 95–110.
[18] H. Fujii, L. Tsang, J. Zhu, K. Nomura, K. Kobayashi, M. Watanabe, Photon transport model for dense polydisperse colloidal suspensions using the radiative transfer equation combined with the dependent scattering theory, Opt. Express 28 (15) (2020) 22962–22977.
[19] H. Fujii, M. Ueno, Y. Inoue, T. Aoki, K. Kobayashi, M. Watanabe, Model equations of light scattering properties and a characteristic time of light propagation for polydisperse colloidal suspensions at different volume fractions, Opt. Express 30 (3) (2022) 3538–3552.
[20] S. Chandrasekhar, Radiative Transfer, Dover, 1960.
[21] K. Furutsu, Y. Yamada, Diffusion approximation for a dissipative random medium and the applications, Phys. Rev. E 50 (5) (1994) 3634–3640.
[22] K.M. Yoo, F. Liu, R.R. Alfano, When does the diffusion approximation fail to describe photon transport in random media? Phys. Rev. Lett. 64 (22) (1990) 2647–2650.
[23] Y. Hoshi, Y. Yamada, Overview of diffuse optical tomography and its clinical applications, J. Biomed. Opt. 21 (9) (2016) 091312 1–11.
[24] Y. Yamashita, T. Hirao, Study on colloidal dispersion systems using dynamic light scattering : Application examples of ELSZ-2000ZS, Univ. Bull. Chiba Inst. Sci. 10 (2017) 43–52.
[25] V.M. Kodach, D.J. Faber, J.V. Marle, T.G.V. Leeuwen, J. Kalkman, Determination of the scattering anisotropy with optical coherence tomography, Opt. Express 19 (7) (2011) 6131–6140.
[26] Z. Zhao, M. Corredig, Colloidal properties of casein micelles suspensions as a function of pH during concentration by osmotic stressing, Food Hydrocoll. 60 (2016) 445–452.
[27] J.D. Cartigny, Y. Yamada, C.L. Tien, Radiative transfer with dependent scattering by particles: Part 1 - theoretical investigation, J. Heat Transf. 108 (1986) 608–613.
[28] C.F. Bohren, D.R. Huffman, Absorption and Scattering of Light By Small Particles, John Wiley & Sons, 1983.
[29] L. Tsang, J.A. Kong, K.-H. Ding, C.O. Ao, Scattering of Electromagnetic Waves: Numerical Simulations, John Wiley & Sons, Ltd, 2001.
[30] J.K. Percus, G.J. Yevick, Analysis of classical statistical mechanics by means of collective coordinates, Phys. Rev. 110 (1) (1958) 1–13.
[31] R.J. Baxter, Ornstein–Zernike Relation and Percus–Yevick approximation for fluid mixtures, J. Chem. Phys. 52 (9) (1970) 4559–4562.
[32] H.J. van Staveren, C.J.M. Moes, J. van Marie, S.A. Prahl, M.J.C. van Gemert, Light scattering in intralipid-10 % in the wavelength range of 400-1100 nm, Appl. Opt. 30 (31) (1991) 4507–4514.
[33] Y. Yamada, H. Suzuki, Y. Yamashita, Time-domain near-infrared spectroscopy and imaging : A review, Appl. Sci. 9 (2019) 1127 1–54.
[34] A.D. Klose, U. Netz, J. Beuthan, A.H. Hielscher, Optical tomography using the time-independent equation of radiative transfer - Part 1 : forward model, J. Quant. Spectrosc. Radiat. Transf. 72 (2002) 691–713.
[35] H. Fujii, S. Okawa, Y. Yamada, Y. Hoshi, Hybrid model of light propagation in random media based on the time-dependent radiative transfer and diffusion equations, J. Quant. Spectrosc. Radiat. Transf. 147 (2014) 145–154.
[36] H. Fujii, M. Ueno, K. Kobayashi, M. Watanabe, Characteristic length and time scales of the highly forward scattering of photons in random media, Appl. Sci. 10 (1) (2020) 93 1–16.
[37] A. Liemert, A. Kienle, Infinite space green's function of the time-dependent radiative transfer equation, Biomed. Opt. Express 3 (3) (2012) 543.
[38] F. Kamran, O.H.A. Abildgaard, A.A. Subash, P.E. Andersen, S. Andersson-Engels, D. Khoptyar, Computationally effective solution of the inverse problem in time-of-flight spectroscopy, Opt. Express 23 (5) (2015) 6937–6945.
[39] H. Fujii, Y. Yamada, G. Chiba, Y. Hoshi, K. Kobayashi, M. Watanabe, Accurate and efficient computation of the 3D radiative transfer equation in highly forward-peaked scattering media using a renormalization approach, J. Comput. Phys. 374 (2018) 591–604.
[40] J.H. Joseph, W.J. Wiscombe, J.A. Weinman, The delta-Eddington approximation for radioactive flux transfer, J. Atmos. Sci. 33 (1976) 2452–2459.
[41] W.G. Egan, T.W. Hilgeman, Optical Properties of Inhomogeneous Materials, Academic, New York, 1979.
[42] H. Fujii, I. Terabayashi, T. Aoki, Y. Inoue, H. Na, K. Kobayashi, M. Watanabe, Numerical study of near-infrared light propagation in aqueous alumina suspensions using the steady-state radiative transfer equation and dependent scattering theory, Appl. Sci. 12 (2022) 1190 1–12.

[43] E. Simon, F. Foschum, A. Kienle, Hybrid green's function of the time- dependent radiative transfer equation for anisotropically scattering semi-infinite media scattering semi-infinite media, J. Biomed. Opt. 18 (1) (2013) 015001 1–6.
[44] M.S. Patterson, B. Chance, B.C. Wilson, Time resolved reflectance and transmittance for the noninvasive measurement of tissue optical properties, Appl. Opt. 28 (12) (1989) 2331–2336.
[45] A. Liemert, A. Kienle, Light diffusion in a turbid cylinder I homogeneous case, Opt. Express 18 (2010) 9456–9473.
[46] A.H. Hielscher, R.E. Alcouffe, R.L. Barbour, Comparison of finite-difference transport and diffusion calculations for photon migration in homogeneous and heterogeneous tissues, Phys. Med. Biol. 43 (1998) 1285–1302.
[47] F. Yi-qiang, F. Xiang, Z. Bin, C. Zheng-dong, S. Zhan, Numerical calculation of apparent IR radiation of cloud, Infrared Phys. Technol. 67 (2014) 84–90.
[48] X. Nie, Q. Mao, Study on shortwave radiative transfer characteristics in polydisperse aerosols in a clear sky, Infrared Phys. Technol. 118 (2021) 103903.
[49] Y. Liu, X. Yang, H. Zhang, C. Guo, F. Huang, Quantitative scattering models of broad-band narrow-beam light through fog, Opt. Express 30 (20) (2022) 35125–35135.
[50] H. Shuai, Z. Jiaqi, L. Shulei, L. Lei, Grid-adaptive Fourier pseudospectral time domain model for the light scattering simulation of atmospheric nonspherical particles, Opt. Express 31 (6) (2023) 10082–10100.